



Research Paper

Tunnelling under pile groups and rafts: Numerical parametric study on tension effects

Y. Hong^a, M.A. Soomro^b, C.W.W. Ng^c, L.Z. Wang^{a,*}, J.J. Yan^a, B. Li^d^a College of Civil Engineering and Architecture, Zhejiang University, China^b Department of Civil Engineering, The Quaid-e-Awam University of Engineering, Science & Technology, Sindh, Pakistan^c Department of Civil and Environmental Engineering, Hong Kong University of Science and Technology, Hong Kong Special Administrative Region^d School of Transportation, Wuhan University of Technology, China

ARTICLE INFO

Article history:

Received 31 October 2014

Received in revised form 21 February 2015

Accepted 22 February 2015

Available online 16 April 2015

Keywords:

Three-dimensional

Numerical parametric study

Hypoplasticity

Tunnelling

Pile group

Piled raft

Tensile force

ABSTRACT

Unfavourable tensile stress can be induced in piles due to tunnelling underneath, as observed in a few recent case histories. Systematic studies of the characteristics of the tunnelling-induced tensile force in pile groups and piled rafts, however, are rarely reported and compared in the literature. Moreover, it remains unclear as to how much working load is required to prevent the axial load in piles from experiencing tension. For this reason, two series (70 runs in total) of three-dimensional finite element analyses (using an advanced soil model) are carried out to simulate tunnelling directly underneath a 2×2 pile group and a 2×2 piled raft in sand. In each series, two variables are considered, namely tunnelling-induced volume loss and working loads acting on the pile cap/raft. The numerical results are verified by two centrifuge tests. It is revealed that due to tunnelling underneath a pile group, the lower part of the piles is dragged downward by the settling soil (by mobilising negative skin friction). The induced dragload (tensile force) is resisted by mobilising positive skin friction (i.e., PSF) along the upper part of the piles. Differing from the pile group, the tunnelling-induced dragload in a piled raft is mostly (up to 75%) resisted by the raft instead of by the PSF. Correspondingly, the neutral plane in the piled raft is located at a shallower depth (with percentage difference up to 36%) than that in a pile group. The maximum tensile stress in the pile group and piled raft is equivalent to 52% and 72% of the tensile strength of concrete, respectively. Larger tensile stress is induced in the piled raft because the raft tends to stop the piles from settling, resulting in larger downward relative soil–pile displacement than that observed in a pile group. To eliminate the tunnelling-induced tension, the working load required for the pile group and the piled raft is up to 73% and 82% of their axial capacity, respectively. The relatively high working load, however, can lead to significant tensile stress (up to 89% of the tensile strength of C50 concrete) at the crown of the tunnel lining.

© 2015 Published by Elsevier Ltd.

1. Introduction

To further develop underground space in congested urban areas, it is unavoidable to construct tunnels directly underneath existing pile foundations [31,12,13,20,21,14,25,22]. Unfavourable tensile stress can be developed in the piles due to tunnelling underneath, as observed by Jacobsz et al. [13], based on field measurement from the Channel Tunnel Rail Link (CTRL) project in the UK. In this project, the 35-km long twin tunnels were constructed under a number of pile supported bridges, as illustrated in Fig. 1. Typical piles (see Pier 7 in Fig. 1(c)) were instrumented to measure changes in their axial strain during tunnelling. The measurements

showed that the tunnelling-induced tensile stress (1.9 MPa) almost reached the ultimate tensile strength of C30 concrete for piles (2 MPa, according to MHUC [19]) when a volume loss of 0.3% was imposed by the tunnelling underneath.

Apart from the field evidence, tunnelling-induced tension in piles was also revealed from numerical analyses [14] and centrifuge model tests [25,26,9]. Lee [14] carried out three-dimensional numerical analyses to simulate tunnel excavation under a single pile and 3×3 and 5×5 groups of piles (without pile cap) in weak weathered rock. The computed results showed that the incremental tensile stress developed in the piles due to tunnelling can be up to 64% of the tensile strength of C30 concrete for piles (i.e., 2 MPa, according to MHUC [19]). Ng et al. [25,26] and Hong et al. [9] reported centrifuge tests simulating tunnelling below a

* Corresponding author.

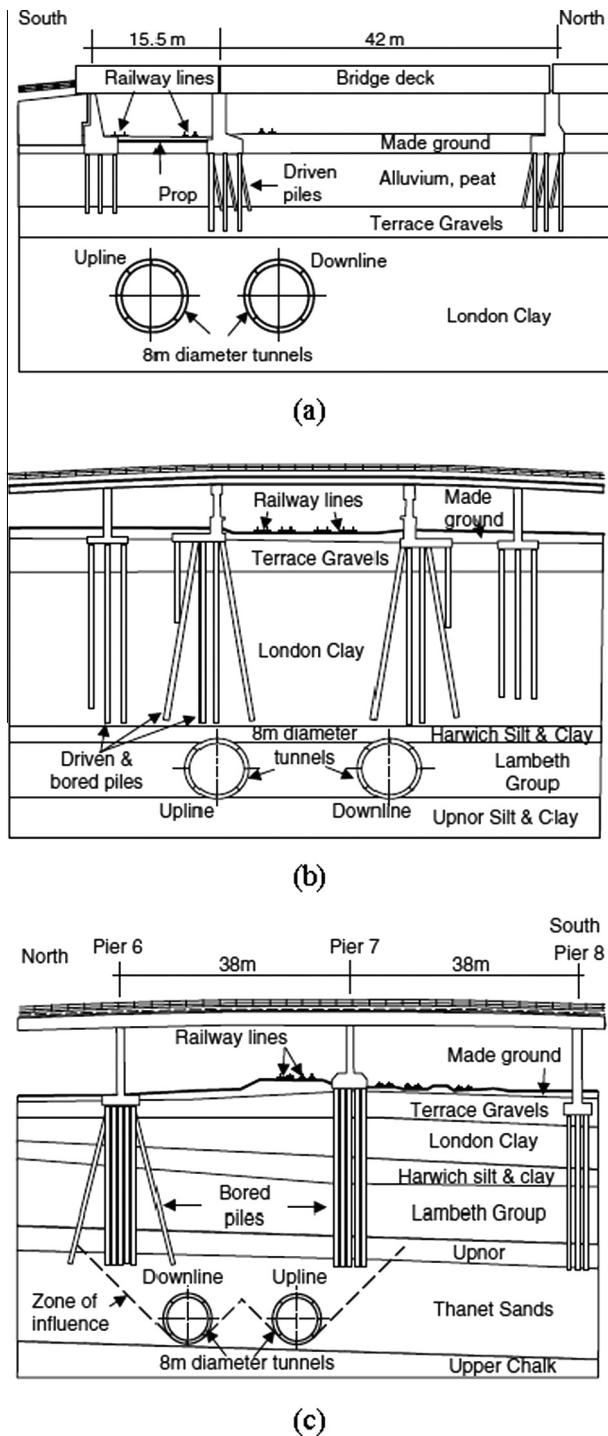


Fig. 1. Three typical sections showing tunnelling under (a) Renwick road bridge; (b) Ripple Road Flyover and (c) A406 viaduct bridge in piled bridges in the Channel Tunnel Rail Link project [13].

2×2 pile group in medium dense sand. Due to the tunnel excavation, substantial incremental tensile stress (up to 50% of the tensile strength of concrete) was also developed in the piles. In spite of the significant incremental tensile force (i.e., reduction in compressive force) caused by tunnelling, the piles are still under compression due to the relatively large working load acting on the pile cap.

Although the aforementioned studies have brought the attention that tension could be developed in piles due to tunnelling underneath, the characteristics (i.e., distribution and magnitude) of tunnelling-induced tensile force in pile groups and piled rafts

have still not been systematically investigated and compared. In addition, it is still unclear how much working load is required to prevent the axial load in the piles from experiencing absolute tension. For these reasons, this study aims to investigate and compare (a) the characteristics of tunnelling-induced tensile force in a pile group and a piled raft, as well as the associated load transfer mechanism and (b) the working load required for a pile group and a piled raft to maintain the piles under compression after tunnelling.

To address the aforementioned objectives, three-dimensional numerical analyses (FEA) are carried out using the commercial finite element software package ABAQUS, which has been widely used to study the effect of tunnelling on existing structures in urban areas [17,23,33,3,15,35,32].

In total, two series of analyses (70 runs in total) are performed to simulate tunnel excavation directly under a pile group and a piled raft. In each parametric study series, two variables are considered, i.e., tunnelling-induced volume loss and working loads acting on the pile cap/raft. In the numerical parametric study, a hypoplastic sand model, which accounts for strain-dependent and path-dependent soil stiffness, is adopted. The hypoplastic model and its model parameters have been calibrated against stress-path triaxial tests and verified through centrifuge tests simulating tunnel–soil interaction in sand [25]. Based on the computed results, the responses of the pile group and the piled raft due to tunnelling underneath are interpreted, compared, and discussed. Calculation charts are developed for estimating the magnitude and location of the maximum tensile stress in pile groups and pile rafts due to tunnelling underneath and for the estimation of working load required to prevent the piles from experiencing tension.

2. Finite element analysis

2.1. Programme of numerical parametric study

Two series (70 runs in total) of numerical analyses were carried out to study the response of a pile group and a piled raft subjected to tunnelling. Each series consists of 35 numerical runs in which various volume losses and working loads acting on the pile group or piled raft are considered. Table 1 summarizes all numerical analyses carried out in this study. The programme of numerical analyses in the table is equally applicable for the scenarios simulating tunnelling underneath a pile group or a piled raft. As shown in the table, the minimum working load adopted in this study (i.e., 1.5 MN), which is meant to represent a load acting on a bridge pier, is determined based on AASHTO LRFD Bridge design specifications

Table 1

A summary of numerical analyses simulating tunnelling underneath a pile group or a piled raft.

Variable	Objective	
Volume loss: %	Working load: MN	
0.3	1.5	Effect of volume loss
0.6		
1.0		
1.5		
2.0		
0.3, 0.6, 1.0, 1.5, 2.0	2.5	Effect of working load
	3.5	
	4.5	
	5.5	
	6.5	
	7.5	

Note: The programme of numerical analyses in the table is equally applicable for the scenarios simulating tunnelling underneath a pile group and a piled raft.

[1]. Apart from the numerical analyses summarised in the table, three additional numerical analyses are carried out to simulate tunnelling in a 'greenfield' and to simulate a loading test of a pile group and a piled raft in a 'greenfield'. The objectives of these three numerical analyses are to obtain the tunnelling-induced settlement trough in a 'greenfield' and the ultimate axial capacity of the pile group and the piled raft.

2.2. Finite element mesh and boundary conditions

Fig. 2 shows an isometric view of a typical finite element mesh (for simulating a piled raft subjected to tunnelling underneath). As illustrated, an existing 2×2 piled raft is located directly above a newly constructed tunnel in medium dense sand (relative density of 65%). The diameter and length of each reinforced concrete pile are 0.8 and 20 m, respectively. The four piles are rigidly connected to a reinforced concrete raft, which has a thickness of 1 m. The tunnel, which is 6 m in diameter (D), is buried at a depth of 22.2 m below the ground surface (i.e., cover over depth ratio = 3.7). The tunnel is 48 m long, equivalent to $8D$. It is excavated in 16 stages, with an advancement distance of $0.5D$ in each stage. The vertical distance between the tunnel crown and the pile toe is approximately $0.4D$ (i.e., 2.2 m). In the numerical analyses simulating a pile group subjected to tunnelling, the embedded depth of each pile and the geometry of the pile cap are identical to those of the piled raft. The elevation height of the pile cap is 4 m above the ground surface.

The lateral and the bottom boundaries of the mesh are fixed using roller and pinned supports, respectively. The mesh consists of 17,732 elements and 20,072 nodes. Eight-node brick elements are used to model the soil, the pile cap, and the deadweight acting on the cap. Four-node shell elements are used to simulate the pile and the tunnel lining. The suitability of the mesh density has been evaluated, by halving the current mesh and re-running the numerical analysis. It is found that halving the computed results based on the full and half mesh size only differ by 2%, suggesting that current mesh is sufficiently fine.

2.3. Constitutive model and model parameters

The basic hypoplastic model was developed to describe the non-linear response of granular materials [34,6]. It consists of eight basic model parameters (ϕ'_c , h_s , n , e_{d0} , e_{c0} , e_{i0} , α and β). The parameters ϕ'_c , h_s , and n denote the effective angle of shearing resistance at the critical state, granular hardness (i.e., pressure-independent stiffness), and an exponent in the power law for one-dimensional compression, respectively. The parameters e_{d0} , e_{c0} , and e_{i0} refer to the minimum void ratio, the maximum void ratio, and the critical void ratio at zero pressure, respectively. The values of α and β govern the dilation angle and shear stiffness of soil, respectively. An increasing α and β means a more dilative and a stiffer soil response, respectively.

To account for the strain-dependency and path-dependency of the soil stiffness (at small strains), Niemunis and Herle [27] further improved the basic hypoplastic model by incorporating the concept of intergranular strain. They introduced five additional parameters: m_R , m_T , R , β_r and χ . The values of R , m_R and m_T control the size of the elastic range, and the initial shear moduli upon 180° and the 90° stress path reversals in the p' - q space (where p' and q represent effective mean normal stress and deviatoric stress), respectively. The remaining two parameters, i.e., β_r and χ , are used to control the shapes of the degradation curves.

The hypoplastic sand model with small strain stiffness has been implemented in the commercial finite element software package ABAQUS [8] through a user-defined subroutine (in umat format),

which is coded in Fortran by P.A. von Wolffersdorff, D. Mašin and C. Tamagnini [5].

In this hypothesised study, the parameters for Toyoura sand were adopted, as the parameters associated with the hypoplastic model of the sand were calibrated and reported by Herle and Gudehus [7] and Ng et al. [25]. The first six model parameters (ϕ'_c , h_s , n , e_{d0} , e_{c0} , e_{i0}) of Toyoura sand were reported by Herle and Gudehus [7]. To obtain the remaining model parameters governing the sand behaviour at large strains (i.e., α and β) and at small strains (i.e., m_R , m_T , R , β_r and χ), Ng et al. [25] carried out stress path triaxial tests for medium density Toyoura sand (relative density = 65%). Four triaxial compression tests were carried out under a constant normal stress (i.e., 100 kPa), considering four different recent stress histories (changes in the direction of stress path $\theta = 0^\circ, 90^\circ, -90^\circ, 180^\circ$). Other details of the stress-path triaxial tests are given by Ng et al. [25]. By calibrating against the measured stress-strain relationship at large strains (deviatoric strain $>1\%$), the best-fit value of α and β were found to be 0.14 and 6, respectively. The five parameters governing path-dependent and strain-dependent soil stiffness were obtained by curve fitting the stiffness degradation curves (at small strains) with different recent stress histories, (i.e., m_R , m_T , R , β_r and χ). In addition to the model parameters, the coefficient of at-rest earth pressure ($K_0 = 0.5$) was estimated based on the effective angle of shearing resistance ($\phi'_c = 31^\circ$, as reported by Ishihara [10]) and Jaky's [11] equation. All model parameters for Toyoura sand are summarised in Table 2. In this study, the effect of spatial variability on soil parameters [16] is not taken into account.

The model pile group, made of an aluminium alloy, was modelled as a linear elastic material with Young's modulus, Poisson's ratio and a unit weight of 70 GPa, 0.2 and 27 kN/m³, respectively.

The soil-pile interface was simulated as elements of zero thickness using duplicated nodes in ABAQUS [8]. This interface was simulated according to the Coulomb friction law, which requires the interface friction coefficient (μ) and limiting displacement (γ_{lim}) to be specified. In this hypothesised study, the μ and γ_{lim} values are assumed to be 0.5 and 2.5 mm, which are typical values for the interface between sand and a rough pile [29]. The interface between the soil-tunnel lining was simulated in the same way as that of the soil-pile interface.

2.4. Procedures of numerical analysis

Each numerical analysis is modelled according to the following procedures:

1. Establish the initial boundary and the initial stress conditions (with $K_0 = 0.5$) of the mesh.
2. Activate the brick elements representing the pile group (modelled as "wished-in-place").
3. Simulate the advancement of the tunnel by specifying zero horizontal displacement at the tunnel face of the first tunnel segment to be excavated. The soil inside of the segment is then 'excavated' by deactivating soil elements inside of it. In the meantime, the shell elements representing the tunnel lining are activated. Before tunnelling, the volume loss is pre-defined by specifying the area of the annulus gap between the tunnel lining and the soil excavated. For example, if a 1% volume loss is intended, the area of soil to be excavated is adjusted, such that the annulus gap between the tunnel lining and the excavating soil is equivalent to a 1% volume loss. The volume loss simulated in this study is therefore independent of other factors, such as the advancement distance of tunnel.
4. Repeat step 3 to excavate the next segment and install the tunnel lining until the completion of the last (16th) segment.

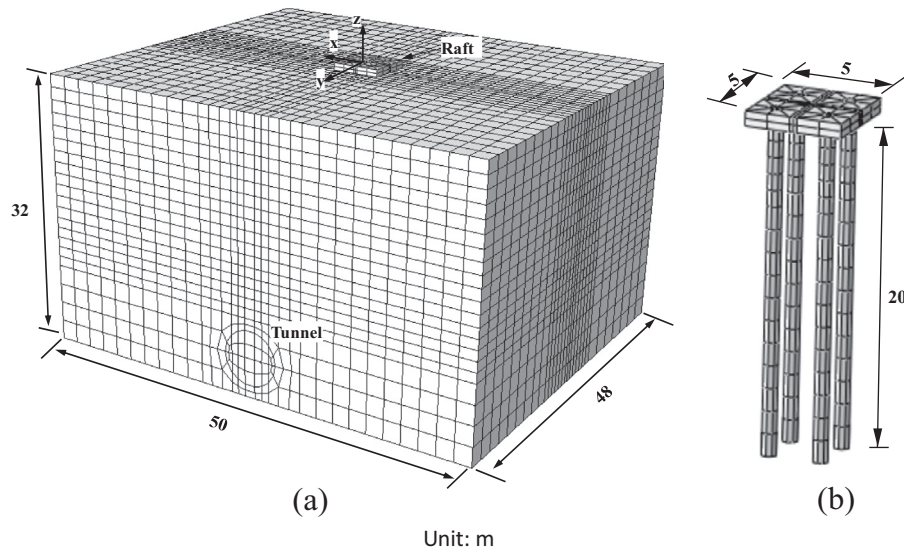


Fig. 2. Finite element mesh of a typical numerical run (i.e., piled raft subjected to tunnelling): (a) full mesh, (b) mesh of the piled raft.

Table 2

Parameters for the hypoplastic sand model adopted in the numerical analyses [25].

Description	Value	Reference
Effective angle of shearing resistance at critical state, ϕ'	31°	Ishihara [10]
Coefficient of at-rest earth pressure, K_0	0.5	Estimated by Jaky's [11] equation
Granular hardness, h_s	2.6 GPa	Herle and Gudehus [7]
Exponent in the power law for one-dimensional compression, n	0.27	
Minimum void ratio at zero pressure, e_{do}	0.61	
Maximum void ratio at zero pressure, e_{lo}	1.10	
Critical void ratio at zero pressure, e_{co}	0.98	
Exponent, α	0.14	Calibrated from stress path triaxial tests by Ng et al. [25]
Exponent, β	6	
Parameter controlling initial shear modulus upon 180° strain path reversal, m_R	11	
Parameter controlling initial shear modulus upon 90° strain path reversal, m_T	6	
Size of elastic range, R	2×10^{-5}	
Parameter controlling degradation rate of stiffness with strain, β_r	0.1	
Parameter controlling degradation rate of stiffness with strain, χ	1.0	

3. Validation of the numerical model

The constitutive model and the model parameters adopted in this study have been validated against three-dimensional centrifuge model tests simulating tunnelling (volume loss = 1%) underneath an existing 2×2 pile group, as reported by Ng et al. [25]. Reasonable agreement was found between the measured and computed results (i.e., settlement and tilting of the pile group, as well as axial load distribution). Due to page constraints, this section only illustrates the validation of the axial load distributions [25], as shown in Fig. 3. All results are shown in prototype scale. The figure shows comparisons between the measured and computed change of axial load in a typical pile (pile P1) in the pile group due to tunnelling at two different locations (i.e., tunnel B and tunnel U, see inset of the figure). In the figure, a negative axial load means a reduction in axial force or the development of net tensile force. It can be observed that the computed change of axial load in both tests reasonably agrees with the measured data, suggesting validity of the hypoplastic model and model parameters adopted in this study.

The measured and computed results in both tests reveal that when there is a tunnel constructed under a pile group, incremental

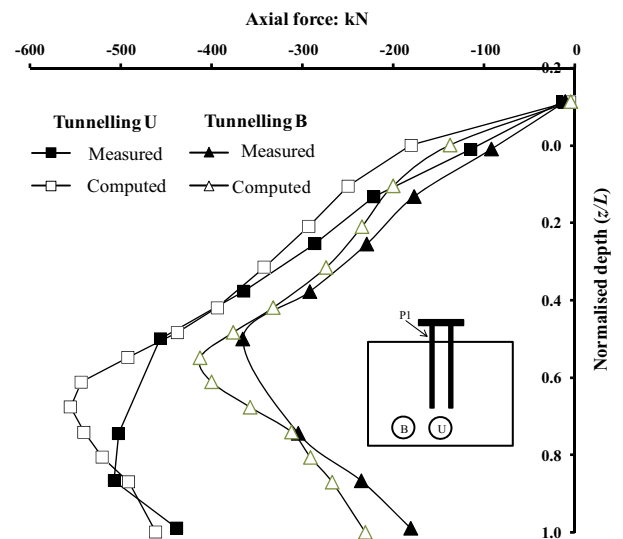


Fig. 3. Comparison between the measured and computed change in axial load in a pile group due to tunnelling [25].

tensile force is developed along the entire length of the pile. The maximum tensile force developed in piles due to tunnelling U (i.e., 507 kN) is larger than that caused by tunnelling B (i.e., 365 kN) because tunnel U is directly located under the pile group. The maximum tunnelling-induced tensile stress (1009 kPa, due to tunnelling U) can be up to approximately 50% of the tensile strength of C30 concrete for piles (2 MPa).

It is worth noting that only three centrifuge tests were carried out by Ng et al. [25]. Therefore, the conclusions drawn by the authors might be relevant only in some specific cases. Moreover, the integrity of the tunnel lining, which is likely to be critical in the cases with high working loads on the piles, was not investigated. In view of these limitations, more systematic parametric studies are carried out in this study to investigate the integrity of both piles and tunnels.

4. Responses of pile group and piled raft with a small working load (bridge pier) to tunnelling

This section focuses on the responses of piled foundations, which are loaded by a small working load (1.5 MN), subjected to tunnelling underneath (volume loss = 1%). This scenario (tunnelling below a bridge pier) is frequently encountered in practical engineering. One typical example is the CTRL project in the UK [13], where tunnels were constructed underneath a number of pile supported bridges (see Fig. 1).

4.1. Pile and ground surface settlement

Fig. 4 shows the tunnelling-induced ground surface settlements in the monitoring section, based on the numerical runs simulating tunnelling in a 'greenfield' (GF), tunnelling underneath a pile group (PG1), and tunnelling under a piled raft (PR1). Both the surface settlement and the transverse distance from tunnel centreline (x) are normalised by the tunnel diameter (D). In the figure, the settlement of piles P1 and P2 (shown in the inset of the figure) are also included for comparison. Moreover, a calculated 'greenfield' settlement trough using a Gaussian distribution [30] is also included for reference. According to Peck [30], the ground surface settlement at an offset x from the tunnel centreline, $S(x)$, can be approximated as

$$S(x) = S_{\max} \exp\left(-\frac{x^2}{2i^2}\right) \quad (1)$$

where S_{\max} is the maximum ground surface settlement and i is the distance from the tunnel centreline to the inflection point of the settlement trough. As proposed by O'Reilly and New [28], i can be represented by KZ , where Z is the vertical distance from the ground surface to the centre of the tunnel, and K is a dimensionless parameter ranging between 0.25 and 0.45 for tunnelling in sand [18]. It is found that a K value of 0.29 results in the best-fitted settlement trough for the 'greenfield' case (GF) in this study.

Although the Gaussian distribution reasonably fits the ground surface settlement in the 'greenfield' case, it underestimates the settlement in the cases featuring the presence of a pile group (i.e., PG1) and of a piledraft (i.e., PR1) by 42% and 53%, respectively. This result suggests that it may be non-conservative to estimate the tunnelling-induced pile settlement based on the 'greenfield' settlement calculated by Gaussian distribution. A similar conclusion was also drawn by Lee [14], based on numerical analyses simulating tunnelling under a group of piles (without pile cap). The larger ground surface settlement induced in the cases with the presence of pile foundations (than that in the 'greenfield') implies that during tunnel excavation, the surface ground is 'dragged' down by the settling piled foundations.

It is also shown that the pile group settles more than that of the ground surface. This downward relative soil–pile movement at the ground surface implies a mobilisation of positive skin friction along the upper part of the pile; evidence is provided in Section 4.3.

Differing from the pile group, the soil underneath the raft settles almost equally with the pile, indicating a full contact between the raft and the surface ground. Due to the raft–soil interaction, the raft tends to prevent the piles from settling, resulting in a settlement less than that of the pile group. Because there is little relative movement between the raft and the surface ground, the mobilised shaft resistance near the upper part of the pile under the raft is likely to be relatively small (illustrated in Section 4.3).

4.2. Distribution of tensile force

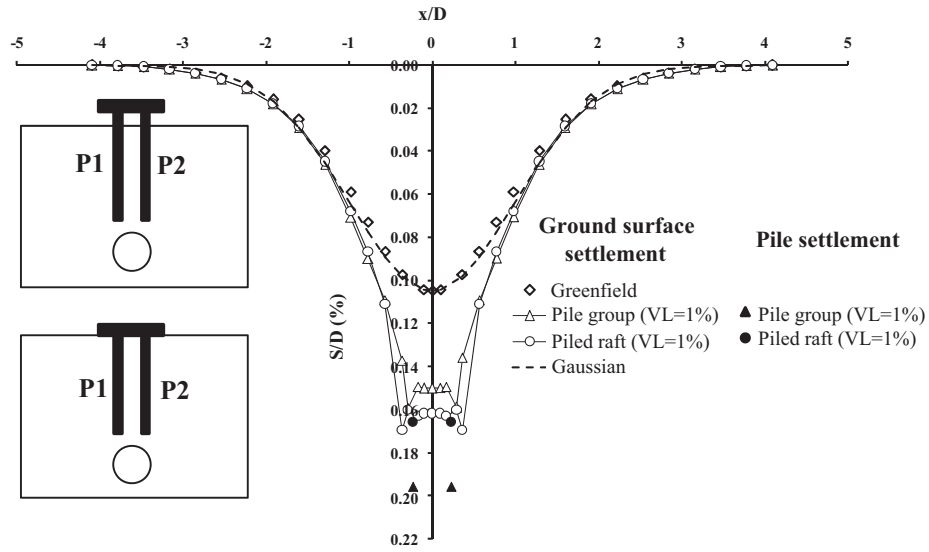
Fig. 5 shows the distribution of the axial load of pile P1 (marked in the inset of the figure), computed from analyses PG1 and PR1, before and after tunnel excavation. In the figure, the depth below the ground surface (Z) is normalised by the pile length (L). A positive axial load means the pile is under compression, and vice versa. Prior to tunnel excavation, the axial load in both the pile group and piled raft reduces with depth due to the mobilisation of positive skin friction, as expected. In the pile group, approximately 79% of the working load acting on the pile cap is resisted by the positive skin friction, while the remaining 21% is supported by toe resistance. In the piled raft, 43% of the working load is resisted by the raft, while the remaining 24% and 33% are supported by the mobilised shaft and toe resistances, respectively.

Due to tunnelling underneath the pile group, the axial load along a great proportion of the pile (i.e., $0.14 < Z/L < 1$) drops below zero, suggesting the development of tensile force. Similar conclusions were also made based on field observation [31] and numerical analyses [14]. Near the pile head (i.e., $0 < Z/L < 0.14$), the axial load remains positive, suggesting that the pile is still under compression, due to the constant working load acting on the pile cap. The maximum induced tensile force in the pile group is 492 kN, which occurs at a depth of $0.61L$ below the ground surface. The corresponding tensile stress (979 kPa) is equivalent to 49% of the tensile strength of concrete (i.e., 2 MPa).

Differing from the response of the pile group, the tensile force is developed along the entire length of the piled raft on completion of tunnelling. A substantial tensile force is developed at the pile head, i.e., 401 kN, which is approximately 62% of the maximum tensile force (642 kN) induced in the pile. This implies that 62% of the 'dragload' is transferred to the raft. This load transfer ratio (tensile force at the raft divided by the maximum tensile force in the pile) can be up to 75%, when the tunnelling-induced volume loss is 0.6%. Due to the soil–raft interaction, a larger 'dragload' and hence larger maximum tensile stress (1278 kPa, equivalent to 64% of the tensile strength of concrete) is developed in the piled raft than that observed in the pile group. Moreover, due to the presence of the raft, the neutral plane (where the maximum tensile force occurs, i.e., at $Z/L = 0.55$) shifts upwards by 16% compared to that in the pile group.

4.3. Mobilised unit shaft resistance

To investigate the load transfer mechanism in the pile group and piled raft due to tunnelling underneath, the mobilised unit shaft resistance is interpreted in this section. Fig. 6 shows the mobilised shaft resistance along pile P1 (marked in the inset of the figure) in the pile group and piled raft, based on the computed results of analyses PG1 and PR1, before and after tunnelling. In the figure, the depth below the ground surface z is normalised by the pile length L . Positive skin friction indicates that the pile settles more than the surrounding soil (i.e., the pile is supporting the soil).



Note: VL denotes volume loss due to tunnelling.

Fig. 4. Settlement of ground and pile foundations (pile group and piled raft) due to tunnelling.

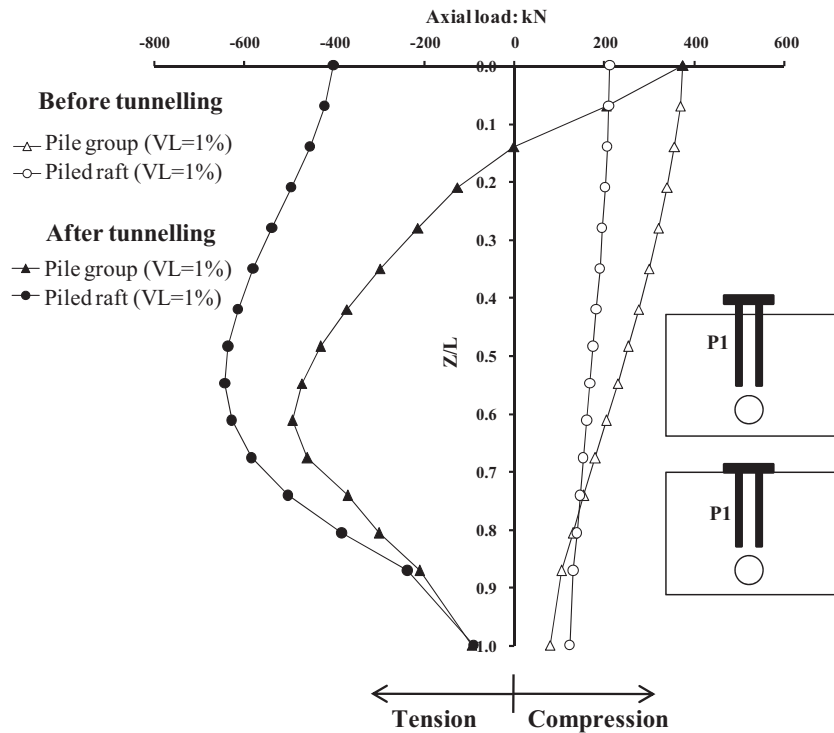


Fig. 5. Axial load distribution.

and vice versa. Referring to the figure, the computed average unit shaft resistance (f_s) mobilised at various depths was calculated based on the following equation:

$$f_s = \frac{\Delta p}{s \Delta z} \quad (2)$$

in which Δp is the difference between the computed axial loads at two consecutive depths, Δz is the vertical distance between the two consecutive depths and s is the perimeter of the pile.

After application of the working load before tunnelling, positive skin friction (PSF) is mobilised along the entire length of the pile

group and the piled raft to support the working load. The average mobilised PSF in the pile group and the piled raft is approximately 22% and 6% of the average ultimate shaft resistance, respectively.

Due to tunnelling under the pile group, negative skin friction (NSF) is mobilised along the lower part of the pile ($0.63 < z/L < 1$), suggesting that this portion of the pile is 'dragged' down by the surrounding soil, which settles due to tunnelling. To maintain vertical equilibrium of the pile, the soil surrounding the upper part of the pile ($0 < z/L < 0.63$) resists it from settling, by mobilising PSF at the soil–pile interface. Consequently, tensile force is induced in the pile (see Fig. 5). The neutral plane, where the zero shaft resistance

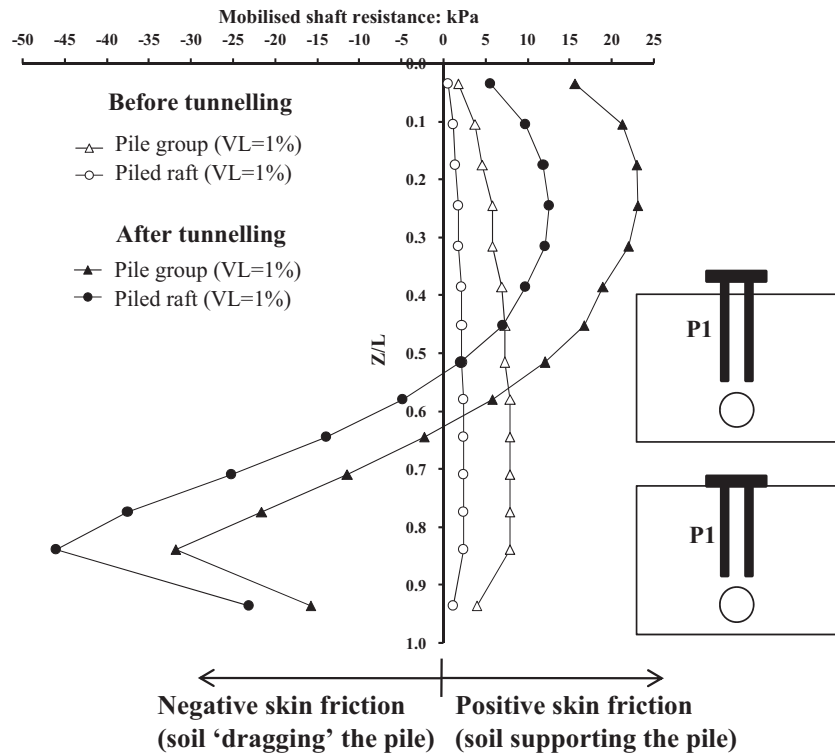


Fig. 6. Mobilised shaft resistance.

is mobilised, is located at a depth of $z/L = 0.63$. This location is consistent with the depth where the maximum axial load occurs (see Fig. 5). Compared with the computed depth neutral plane (NP) in this study ($z/L = 0.63$), the NP reported by Lee [14] was located at a much deeper depth (z/L ranging from 0.87 to 0.9), based on numerical analyses of tunnelling below a group of piles, with a configuration of 3×3 or 5×5 (without pile cap) in weathered rock. This difference can be attributed to a number of reasons, such as the larger stiffness of the soil and greater number of piles adopted in Lee [14]'s study, compared to those in this study. After tunnelling, full mobilisation of shaft resistance is achieved near the pile head ($z/L = 0$).

Compared to the pile group, a much smaller PSF (approximately 50% less) is mobilised near the upper part of the piled raft ($0 < z/L < 0.55$). In contrast, a larger NSF is mobilised at the lower part of the piled raft ($0.55 < z/L < 1$) than that mobilised in the pile group. Due to tunnelling underneath, full mobilisation of unit shaft resistance is achieved near the toe of the piled raft ($z/L = 0$). This is distinctively different from the pile group, in which full mobilisation of shaft resistance occurs near the pile head. It is worth noting that for each pile under the raft, the resultant force of the mobilised PSF is only 38% of that caused by the mobilised NSF. In other words, only 38% of the dragload (due to NSF) is resisted by the resultant force of the PSF. The remaining 62% of the dragload is transferred to the raft, leading to significant tension at the pile head (see Fig. 5). The presence of the raft also results in an upward shift (by 16%) of the NP when compared with piles in the group. This means that due to the contribution from the raft, a lesser proportion of the pile is required to resist the dragload (by mobilising PSF), resulting in a shallower depth of NP.

4.4. Relative shear displacement at the soil–pile interface

To further interpret the tunnelling-induced shear transfer mechanism in the pile group and piled raft, Fig. 7 shows the distributions of the relative soil–pile settlement (before and after

tunnel excavation) computed from analyses PG1 and PR1. A positive relative soil–pile settlement means that the soil settles less than the pile (i.e., the pile is supporting the soil), and vice versa.

Due to the application of the working load (prior to tunnelling) in both the pile group and the piled raft, each pile settles more than its surrounding soil along the full pile depth, as expected. This confirms the mobilisation of PSF, as shown in Fig. 6. The distributions of relative soil–pile settlement, however, are altered significantly after tunnelling underneath the pile foundations. For the pile group, positive relative soil–pile settlement is developed along the upper part of the pile ($0 < z/L < 0.62$), while the direction of the relative settlement reverses from positive to negative at the lower part of the pile ($0.62 < z/L < 1$). This indicates that the soil surrounding the lower portion of the pile drags the pile down, while the soil adjacent to the upper portion of the pile resists pile settlement, leading to tensile force in the pile. The largest relative soil–pile settlement (i.e., 2.9 mm) is developed near the pile head ($z/L = 0$), exceeding the limiting relative soil–pile displacement (i.e., 2.5 mm). The shaft resistance near the pile head is therefore fully mobilised, as discussed in the previous section. The computed results reported by Lee [14] also show that while a group of piles (without cap) was subjected to tunnelling underneath, the largest relative soil–pile displacement was developed near the pile head.

Compared to the pile group, much less (approximately 60% less) positive soil–pile settlement is developed along the upper part ($0 < z/L < 0.55$) of the pile under the raft. This is because of the full-contact between the raft and the soil underneath (as illustrated in Fig. 4), such that the soil underneath the raft tends to settle with the pile as a block, as noted by Fleming et al. [4]. Consequently, the PSF mobilised along the upper portion of the piled raft is substantially less than that in the pile group (as shown in Fig. 6). However, larger negative relative soil–pile settlement is developed along the lower part ($0.55 < z/L < 1$) of the piled raft than in the pile group. This is because the raft tends to stop the piles underneath from settling (as revealed by Fig. 4), such that the soil near the lower portion of the pile settles more in relation to the

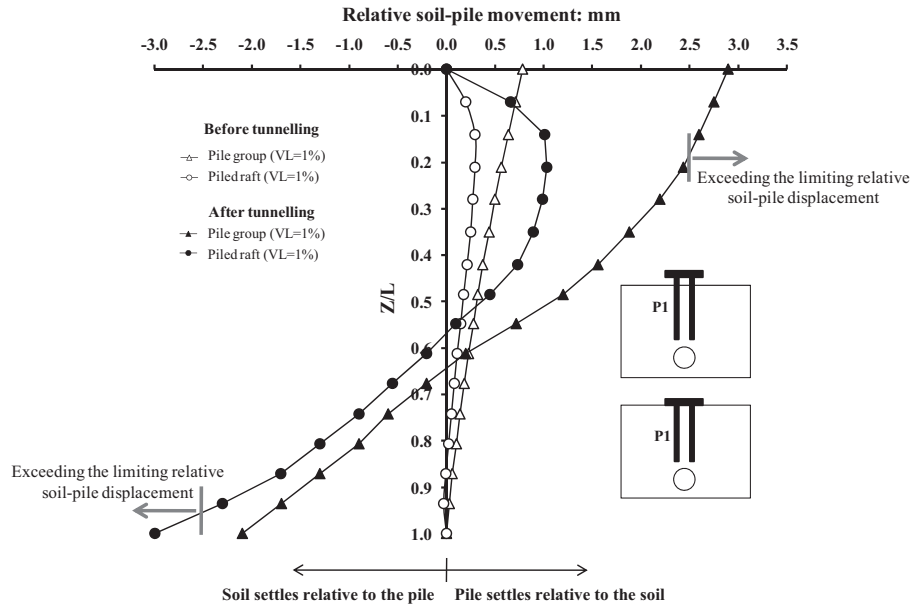


Fig. 7. Relative shear displacement at the soil-pile interface.

pile, compared to the pile group. Consequently, the lower portion of the pile under the raft experiences more NSF than the pile group. The most significant relative soil-pile settlement (i.e., 3 mm), which exceeds the limiting relative soil-pile displacement (2.5 mm), is developed near the toe of the piled raft ($z/L = 1$). Full mobilisation of shaft resistance is therefore achieved near toe of the piled raft, as discussed in the previous section.

4.5. Effect of volume loss on magnitude and location of the maximum tensile stress

To assist with the engineering design for piles under which there is a potential to construct new tunnels, it is necessary to estimate the magnitude ($\sigma_{T-\max}$) and the location (i.e., depth of neutral plane, z_{np}) of the maximum tensile stress induced in the piles. Calculation charts are therefore developed, based on the numerical parametric study reported herein, for estimating $\sigma_{T-\max}$ and z_{np} at various volume losses.

Fig. 8 shows the relationship between volume loss and normalised maximum tensile stress (i.e., $\sigma_{T-\max}/\sigma_t$, where σ_t is the

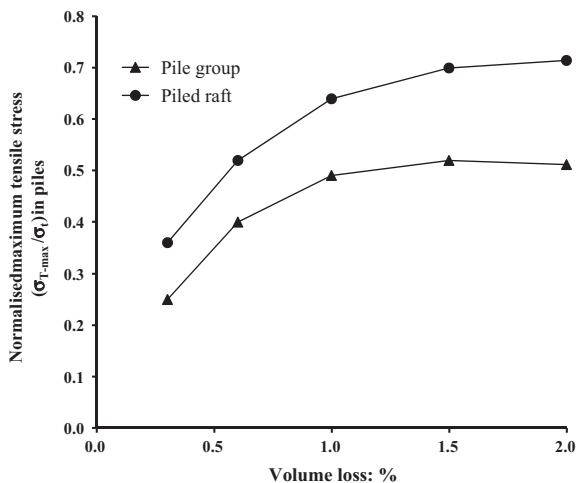


Fig. 8. A calculation chart for estimating the maximum tensile stress in the pile group and piled raft.

tensile strength of concrete, 2 MPa) in the pile group and the piled raft. For the pile group, the maximum tensile stress in the piles increases with volume loss (VL) until the VL reaches 1.5%. As the volume loss is further increased, the maximum tensile stress in the piles decreases slightly. Differing from the pile group, the maximum tensile stress developed in the piled raft continues to increase with volume loss at a decreasing rate. Explanations of the two different trends for the pile group and piled raft are given in the latter part of this section. The tunnelling-induced tensile stress developed in a piled raft is always larger than that in a pile group at a given volume loss, with a maximum percentage difference of 44% between the two. This is because the presence of the raft tends to prevent the pile from settling, leading to larger downward relative soil-pile settlement in the lower portion of the pile and hence larger tensile stress in the pile. Based on the conditions simulated, the maximum tensile stress in a pile group and a piled raft resulting from the tunnelling underneath can be up to 72% and 52% of the tensile strength of C30 concrete (i.e., 2 MPa, according to MHUC [19]) for piles, respectively.

Fig. 9 shows the relationship between the normalised depth where the maximum tensile stress develops in piles (i.e., z_{np}/L)

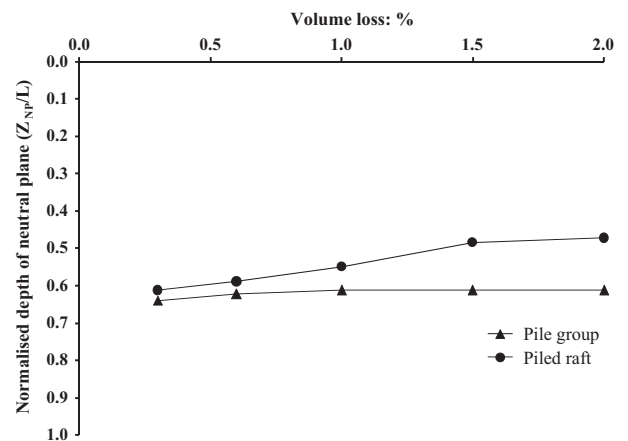


Fig. 9. A calculation chart for estimating depth of the maximum tensile stress (i.e., depth of neutral plane) in the pile group and piled raft.

and the tunnelling-induced volume loss. It can be observed that the location of the neutral plane is relatively independent of volume loss, suggesting that the total area of NSF does not change with increased volume loss. The normal stress acting on the lower portion of the pile, however, decreases with volume loss when it exceeds 1.5% (due to stress release). As a result, the NSF mobilised along the pile shaft and hence the maximum tensile stress developed in the pile decreases slightly when the volume loss becomes larger than 1.5% (Fig. 8). Differing from the piled group, the location of the neutral plane in the piled raft moves upward as the volume loss increases. This is because the settlement of the soil increases with volume loss while the settlement of the piled raft is suppressed due to the raft–soil interaction. Consequently, more areas of the pile shaft are subjected to downward soil movement as the volume loss increases, leading to an increased dragload and hence tensile stress in the piled raft (Fig. 8).

5. Effect of working load on tunnelling-induced axial response in the pile group and piled raft

The previous section focuses on the development of tunnelling-induced tensile force in pile foundations with a small working load (such as in a bridge pier). This represents the worst case scenario, in terms of tunnelling-induced tensile force. Apart from this scenario (a pile supported bridge pier), pile foundations are usually axially loaded by a certain amount of working load, which may prevent the pile foundations from experiencing tension when subjected to tunnelling underneath. This section aims to investigate and quantify the effects of working load on the tunnelling-induced axial load distribution in a pile group and a piled raft.

Fig. 10(a) compares the distribution of axial load in a pile group loaded by various working loads after tunnelling (volume loss = 1%). Each working load is normalised by the ultimate axial capacity (i.e., $P_{ul} = 8.6$ MN) of the pile group. The axial capacity is determined based on the computed load–settlement curve of the pile group (by a numerical pile loading test in the ‘greenfield’ case) and the settlement acceptance failure criterion proposed by Ng et al. [24]. It is revealed that the maximum tensile force decreases as the working load increases, with the location of NP shifting downward. When the applied working load reaches $0.69P_{ul}$, the tensile force and mobilised NSF in the pile group are completely eliminated, with the NP located near the pile toe ($z_{np}/L = 0.8$).

Fig. 10(b) shows the distribution of the axial load in piled rafts loaded by various working loads on the completion of the tunnelling. Each working load is normalised by the ultimate axial capacity (i.e., $P_{ul} = 10.1$ MN) of the piled raft, which is determined according to the computed results of the pile loading test on the piled raft and the settlement acceptance failure criterion proposed by Ng et al. [24]. It can be observed that an increase of the working load applied to the piled raft results in a reduction of the tensile force in the piles and a downward shift of the neutral plane. This trend is similar to the pile group. The working load required to prevent the piled raft from experiencing tension is 7.5 MN, which is equivalent to $0.74P_{ul}$. This ratio is larger than that required for the pile group (i.e., 0.69). A larger load is required to eliminate tension in a piled raft because the working load is not only transferred to the soil–pile interface for elimination of negative skin friction but is also transferred to the contact surface between the raft and the soil.

To quantify the minimum working load (P_{wl}) needed to prevent the pile group and piled raft from experiencing tension caused by tunnelling at various volume losses, a calculating chart was developed (shown in Fig. 11) based on the parametric study. In the chart, P_{wl} is normalised by the ultimate axial capacity of the pile group or the piled raft. It can be observed that for the pile group, P_{wl}/P_{ul}

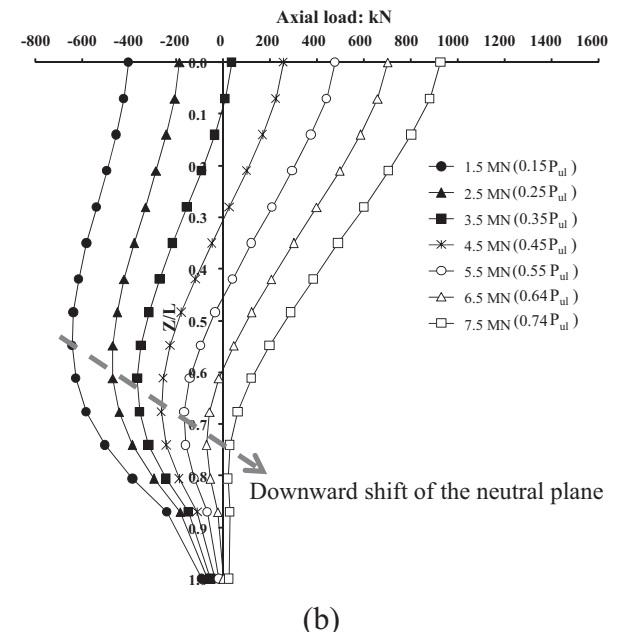
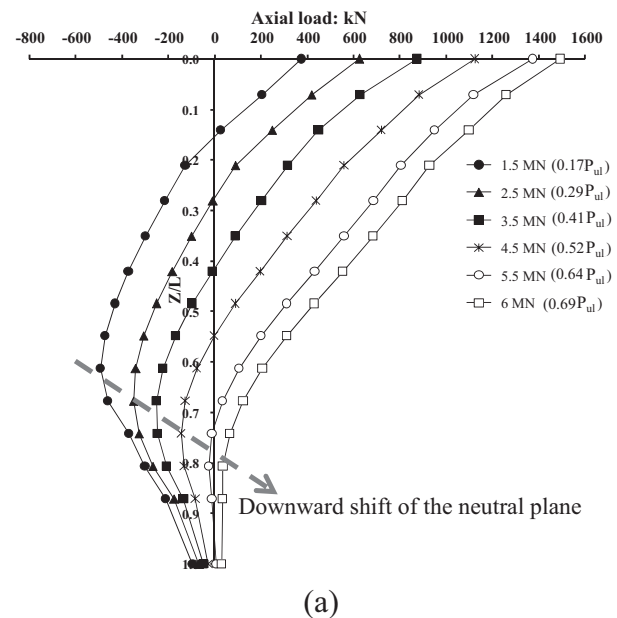


Fig. 10. Effect of working load on axial load distribution in the (a) pile group and (b) piled raft subjected to tunnelling underneath (volume loss = 1%).

increases with volume loss until it reaches 1.5%. When the volume loss exceeds 1.5%, there is a slight reduction in P_{wl}/P_{ul} . However, P_{wl}/P_{ul} for the piled raft keeps increasing with volume loss, at a decreasing rate. These relationships are consistent with the relationships between the induced maximum tensile stress in piles and volume loss (Fig. 8). Based on the cases considered in this study, the minimum working load required to prevent the occurrence of tension in a pile group and a piled raft is in the ranges 38–73% and 44–82% of their ultimate axial capacities, respectively, depending on the volume loss.

6. Integrity of tunnel lining

In the previous section, it is illustrated that by increasing the working load applied to the pile cap/raft, the tunnelling-induced tension in the piles can be eliminated. The high working load

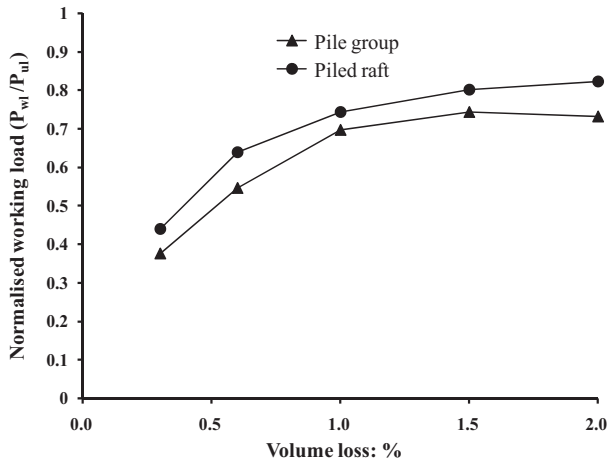


Fig. 11. A calculation chart for estimating the minimum working load required to prevent the piles from experiencing tension after tunnelling.

applied to the pile foundations, however, can impose additional loading to the tunnel lining located underneath the piles, as noted by Lee [14]. This section aims to explore the influence of working load (applied to piles) on the integrity of the tunnel lining.

Fig. 12(a) shows the induced bending moment of tunnel linings (on completion of tunnel excavation) in two worst case scenarios,

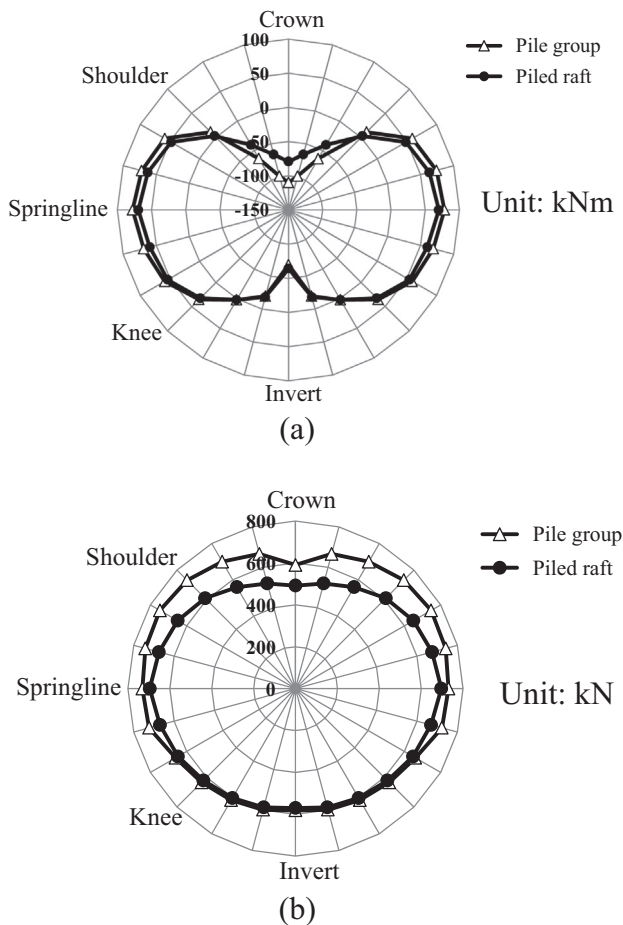


Fig. 12. (a) Bending moment and (b) axial load in the tunnel lining after tunnel excavation with a 0.3% volume loss underneath pile foundations vertically loaded by 7.5 kN.

where the pile group and piled raft are loaded by the largest working load considered in this study (i.e., 7.5 MN) and the smallest volume loss (i.e., 0.3%) is induced. In the figure, positive bending moment denotes a hogging moment (with tension induced on the outer side of the tunnel lining), while negative bending moment refers to a sagging moment (with tension developed on the inner side of the tunnel lining). As expected, the distribution of the bending moment in the tunnel linings underneath the pile group and piled raft is symmetrical with respect to the centreline of the lining. In both cases, a hogging bending moment is developed at the crown and the invert, while a sagging bending moment is induced at the springlines. It can be observed that the major differences of the bending moment between the two cases occur near the crown of the linings. At the crown of the lining underneath the pile group, a bending moment of 79 kN m is developed, being 38% larger than that in the tunnel lining underneath the piled raft. This is because under the same working load, larger toe resistance is mobilised in the pile group than in the piled raft, such that the lining under the pile group is subjected to a larger load.

Fig. 12(b) shows the axial load developed in the tunnel linings under the pile group and the piled raft. In the figure, a positive axial load means the section is under compression. It can be observed that for the linings under both the pile group and piled raft, compression is induced along the full cross section. The major difference in the axial load of the lining between the two cases occurs in the region from the shoulder to the springline. As expected, larger maximum axial load is induced in the lining underneath the pile group than under the piled raft, with a maximum percentage difference of 27% between the two.

Based on the computed bending moment and axial load shown in Fig. 12, tensile stress developed in the tunnel lining can be readily calculated. The calculation shows that the maximum tensile stress in both cases is developed at the crown of the tunnel lining. For the tunnels under the pile group and the piled raft loaded with a working load of 7.5 MN, the maximum tensile stresses developed at the crown of the lining are 3.4 and 4.9 MPa, respectively. These two values are equivalent to 61% and 89% of the tensile strength of the concrete with grade C50 for tunnel lining [i.e., tensile strength = 5 MPa, according to ACI [2]]. By considering different volume losses, the maximum tensile stresses developed at the crown of the tunnel lining under the pile group and the piled raft (under the maximum working load, i.e., 7.5 MN) are shown in Fig. 13. It can be observed that for the tunnel lining under both the pile group and piled raft, the maximum tensile stress in the lining decreases with increasing volume loss. This occurs because an increasing volume loss leads to a reduction of the toe resistance of the piles, leading to a decrease in soil pressure above the crown

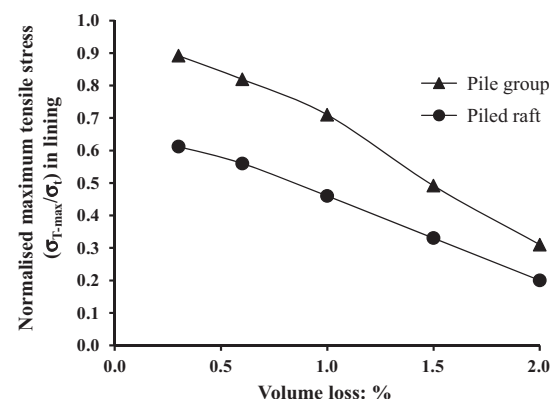


Fig. 13. Development of tensile stress at the crown of the tunnel lining after tunnel excavation with various volume losses.

of the lining. For the tunnel lining positioned underneath the pile group, the maximum tensile stress (developed at crown) ranges from 30% to 89% of the tensile strength of C50 concrete. Comparatively, smaller tensile stress is developed in the lining under the piled raft, in the range between 20% and 61% of the tensile strength of C50 concrete.

7. Summary and conclusions

In this study, two series (70 runs in total) of finite element analysis are carried out to investigate and compare the characteristics of tensile force developed in a 2×2 pile group and a 2×2 piled raft due to tunnelling directly under the pile foundations in medium density sand. Various volume losses and working loads are considered in the numerical parametric study. Based on the ground conditions, dimensions and locations of the pile foundations and tunnels simulated, the following conclusions can be drawn:

- (1) Due to the presence of the pile group and the piled raft, the tunnelling-induced ground surface settlements are approximately 42% and 53% larger than those developed in a 'greenfield'. This suggests that it may be non-conservative to estimate tunnelling-induced pile settlement based on the 'greenfield' settlement calculated by a Gaussian distribution.
- (2) When a tunnel is excavated under a pile group (with a small working load), the soil surrounding the lower portion ($0.61 < z/L < 1$, where z and L denote the depth below the ground surface and the pile length, respectively) of the piles settles more than the pile, 'dragging' down the piles by mobilising negative skin friction. The 'dragload' is resisted by mobilising positive skin friction along the upper portion ($0 < z/L < 0.61$) of the piles. Tensile force is therefore developed in the piles.
- (3) Differing from the load transfer mechanism in the pile group, the 'dragload' developed in the lower portion of the piled raft is mostly (up to 75%) transferred upward to the raft, rather than resisted by mobilising positive skin friction along the upper portion of the pile. As a result, a lesser proportion of the pile under the raft is subjected to positive skin friction when compared with that in the pile group. In other words, the presence of the raft leads to an upward shift of the neutral plane (NP). At each given volume loss, the NP of the piled raft is always located at a shallower depth than that of the pile group, with a percentage difference up to 36%.
- (4) The tunnelling-induced tensile stress developed in a piled raft is always larger than that in a pile group at various volume losses, with a maximum percentage difference of 44% between the two. This is because the presence of the raft reduces the settlement of the piles, leading to a larger downward relative soil–pile settlement along the lower portion of the pile and hence a larger tensile stress in the pile. The maximum induced tensile stress in the pile group and the piled raft is up to 52% and 72% of the tensile strength of C30 concrete for piles (2 MPa), respectively.
- (5) On completion of tunnelling, the most significant percentage mobilisation of shaft resistance in a pile group occurs near the pile head. In contrast, shaft resistance in a piled raft is most substantially mobilised near the pile toe. The presence of the raft, which tends to prevent the pile from settling, suppresses the development of upward relative soil–pile movement near the upper portion of the pile and magnifies downward relative soil–pile movement near the lower portion of the pile.

- (6) As the working load acting on the pile group or the piled raft increases, the absolute tensile stress in the piles after tunnelling decreases, accompanied by a downward shift of the NP. To prevent the pile foundations above the tunnelling from experiencing absolute tension after tunnelling, the minimum working load (P_{wl}) required for the pile group and the piled raft is approximately 38–73% and 44–82% of their ultimate axial capacity, depending on the amount of volume loss. A calculation chart, which correlates P_{wl} to volume loss for both the pile group and the piled raft, was developed.
- (7) Although an increase of working load at the pile cap/raft can help eliminate tension in piles, it imposes additional loads to the tunnel lining underneath the pile group and the piled raft. Due to the relatively high working load on piles, tensile stress is developed near the crown of the tunnel lining. Based on the scenarios considered in this study, the maximum induced tensile stress in tunnel linings under the pile group and the piled raft can be up to 61% and 89% of the tensile strength of C50 concrete for tunnel lining, respectively.

It is worth noting that all the conclusions drawn in this study are made from numerical analyses simulating tunnelling in dry sand, where effect of ground water is ignored. Any extrapolation of the conclusions should be treated with caution.

Acknowledgements

The authors gratefully acknowledge the financial support provided by the Research Grants Council of the HKSAR (General Research Fund Projects No. 617511), International S&T Cooperation Program of China (Grant no. 2015DFE72830), the Quaid-e-Awam University of Engineering, Science & Technology, Sindh and Pakistan, the National Natural Science Foundation of China (Project No. 51408540), Distinguished Young Scholars of China (Grant No. 51325901) and State Key Program of National Natural Science of China (Grant No. 51338009).

References

- [1] AASHTO LRFD Bridge. Bridge design specifications. U.S.: American Association of State Highway Officials; 2012.
- [2] ACI. Control of cracking in concrete structures (ACI 224R-01). MI: American Concrete Institute (ACI); 2001.
- [3] Chungsik Y. Interaction between tunneling and bridge foundation – a 3D numerical investigation. *Comput Geotech* 2013;49:70–8.
- [4] Fleming W GK, Weltman AJ, Randolph WF, Elson WK. *Piling engineering*. 3rd ed. Blackie Academic & Professional; 2008.
- [5] Gudehus G, Amorosi A, Gens A, Herle I, Kolymbas D, Mašin D, et al. The soilmodels.info project. *Int J Numer Anal Meth Geomech* 2008;32(12):1571–2.
- [6] Gudehus G, Mašin D. Graphical representation of constitutive equations. *Geotechnique* 2009;59(2):147–51.
- [7] Herle I, Gudehus G. Determination of parameters of a hypoplastic constitutive model from properties of grain assemblies. *Mech Cohes Frict Mater* 1999;4: 461–86.
- [8] Hibbitt, Karlsson & Sorensen Inc. ABAQUS user's manual, version 6.8.2; 2008.
- [9] Hong Y, Soomro MA, Ng CWW. Settlement and load transfer mechanism of a pile group due to side-by-side twin tunneling. *Comput Geotech* 2015;64: 105–19.
- [10] Ishihara K. Liquefaction and flow failure during earthquakes. *Geotechnique* 1993;43(3):351–415.
- [11] Jáky J. The coefficient of earth pressure at rest. *J Soc Hung Archit Eng* 1944;355–8 [in Hungarian].
- [12] Jacobsz SW, Standing JR, Mair RJ, Hahiwara T, Suiyama T. Centrifuge modeling of tunnelling near driven piles. *Soil Found* 2004;44(1):51–8.
- [13] Jacobsz SW, Bowers KH, Moss NA, Zanardo G. The effects of tunnelling on piled structures on the CTRL. In: *Geotechnical aspects of underground construction in soft ground*. Proceedings of the 5th international symposium TC28. Amsterdam, the Netherlands, 15–17 June 2005; 2006.
- [14] Lee CJ. Three-dimensional numerical analyses of the response of a single pile and pile groups to tunnelling in weak weathered rock. *Tunn Undergr Space Technol* 2012;32:132–42.
- [15] Liu C, Zhang Z, Regueiro RA. Pile and pile group response to tunnelling using a

- large diameter slurry shield – case study in Shanghai. *Comput Geotech* 2014; 59:21–43.
- [16] Li DQ, Qi XH, Zhou CB, Phoon KK. Effect of spatially variable shear strength parameters with linearly increasing mean trend on reliability of infinite slopes. *Struct Saf* 2014;49:45–55.
- [17] Liu HY, Small JC, Carter JP, Williams DJ. Effects of tunnelling on existing support systems of perpendicularly crossing tunnels. *Comput Geotech* 2009;36(5):880–94.
- [18] Mair RJ, Taylor RN. Bored tunnelling in the urban environment. State-of-the-art report and theme lecture. *Proceedings of 14th international conference on soil mechanics and foundation engineering*, vol. 4. Hamburg: Balkema; 1997. p. 2353–85.
- [19] MHUC. Code for design of concrete structure, GB50010–2010. China: The Ministry of Housing and Urban-Rural Construction; 2010.
- [20] Marshall AM, Mair RJ. Tunneling beneath driven or jacked end-bearing piles in sand. *Can Geotech J* 2011;48(12):1757–71.
- [21] Marshall AM. Tunnel–pile interaction analysis using cavity expansion methods. *ASCE J Geotech Geoenviron Eng* 2012;138(10):1237–46.
- [22] Marshall AM, Twana H. An analytical study of tunnel–pile interaction. *Tunn Undergr Space Technol* 2015;45:43–51.
- [23] Migliazza M, Chiorboli M, Giani GP. Comparison of analytical method, 3D finite element model with experimental subsidence measurements resulting from the extension of the Milan underground. *Comput Geotech* 2009;36(1–2):113–24.
- [24] Ng CWW, Yau TLY, Li JHM, Tang WH. New failure load criterion for large diameter bored piles in weathered geomaterials. *J Geotech Geoenviron Eng, ASCE* 2001;127(6):488–98.
- [25] Ng CWW, Hong Y, Soomro MA. Effects of piggyback twin tunnelling on a pile group: three-dimensional centrifuge and numerical modelling. *Géotechnique* 2014;65(1):38–51.
- [26] Ng CWW, Soomro MA, Hong Y. Three-dimensional centrifuge modelling of pile group responses to side-by-side twin tunneling. *Tunn Undergr Space Technol* 2014;43:350–61.
- [27] Niemunis A, Herle I. Hypoplastic model for cohesionless soils with elastic strain range. *Mech Cohes-Frict Mater* 1997;2:279–99.
- [28] O'Reilly MP, New BM. Settlements above tunnels in the United Kingdom—their magnitude and prediction. In: *Proceedings of the conference tunnelling'82*, IMM, London; 1982. p. 173–81.
- [29] Peng SY. Influence of stress relief due to deep excavation on capacity of pile foundations. PhD thesis, Hong Kong University of Science and Technology; 2012.
- [30] Peck RB. Deep excavations and tunneling in soft ground. In: *Proceeding of the 7th international conference on soil mechanics and foundation engineering*. Sociedad Mexicana de Mecanica de Suelos, A.C., Mexico City; 1969. p. 225–90.
- [31] Selemetas D. The response of full-scale piles and piled structures to tunnelling. PhD thesis, University of Cambridge; 2005.
- [32] Soomro MA, Hong Y, Ng CWW, Lu H, Peng SY. Load transfer mechanism in pile group due to single tunnel advancement in stiff clay. *Tunn Undergr Space Technol* 2015;45:63–72.
- [33] Svoboda T, Mašín D, Boháč J. Class A predictions of a NATM tunnel in stiff clay. *Comput Geotech* 2010;37(6):817–25.
- [34] von Wolfersdorff PA. A hypoplastic relationship for granular materials with a predefined limit state surface. *Mech Cohes-Frict Mater* 1996;1:251–71.
- [35] Zhang Z, Huang M. Geotechnical influence on existing subway tunnels induced by multiline tunneling in Shanghai soft soil. *Comput Geotech* 2014;56:121–32.